Available online at www.sciencedirect.com
ScienceDirect
Journal of Electroanalytical Chemistry 599 (2007) 194–202
Journal of Electroanalytical Chemistry
www.elsevier.com/locate/jelechem

Preparation of nanostructures composed of dextran sulfate/ruthenium nanoparticles and their interaction with phospholipid monolayers at a liquid–liquid interface

Hélder A. Santos [a,*], Vladimir García-Morales [b], Lasse Murtomäki [a], José A. Manzanares [b], Kyösti Kontturi [a,*]

[a] *Department of Chemical Technology, Laboratory of Physical Chemistry and Electrochemistry, Helsinki University of Technology, P.O. Box 6100, Kemistintie 1, FIN-02015 HUT Espoo, Finland*
[b] *Departament de Termodinàmica, Universitat de València, C/Dr. Moliner 50, E-46100 Burjassot, Spain*

Received 19 October 2005; received in revised form 10 January 2006; accepted 18 January 2006
Available online 20 March 2006

Abstract

Nanostructures composed of dextran sulfate (DS)/ruthenium (Ru) nanoparticles (NPs) adsorbed on phospholipid monolayers at a liquid–liquid interface were prepared and characterized electrochemically in relation to their potential use in drug delivery systems. First, positively charged Ru NPs were prepared, and then negatively charged DS was adsorbed on the surface of the NPs, thus forming well-defined and organized structures, as observed under the transmission electron microscope, which are referred to composite nanoclusters. The lipid monolayers were formed by depositing either 1-palmitoyl-2-oleoyl-*sn*-glycero-3-phosphatidylcholine or 1-palmitoyl-2-oleoyl-*sn*-glycero-3-phospho-*rac*-(1-glycerol) at an air–liquid interface with an aqueous subphase containing calcium chloride and the composite nanoclusters. Using the Langmuir–Blodgett technique, the lipid monolayers were transferred onto an immobilized organic gel at different surface pressures (32, 40, and 47 mN/m) and their physicochemical properties were studied by compression π–A isotherms and capacitance–potential curves. All the relevant changes in these latter curves were successfully explained with a theoretical model and were ascribed to a reduced surface charge density at the interface after the adsorption of the composite nanoclusters. The transfer mechanism of two ionisable compounds of pharmaceutical interest, the Alzheimer drug tacrine (9-amino-1,2,3,4-tetrahydroacridine hydrochloride) and the therapeutic anti-infective dye aminacrine (9-aminoacridine hydrochloride), across these interfacial composite nanostructures was then studied by cyclic voltammetry. It was demonstrated that the lipid layer retards the rate of ion transfer.

Keywords: Dextran sulfate/ruthenium nanoparticles; Phospholipid monolayers; Liquid–liquid interface; Drug delivery; Capacitance curves; Cyclic voltammetry

1. Introduction

Glycosaminoglycans (GAGs) are acidic unbranched polysaccharides that exhibit a variety of different biological activities. These polymers are constituted by repeated dimers of hexuronic acid and a hexosamine both linked by β-1,3-glycosidic bonds. Their biological properties are mostly expressed by interactions with plasma and tissue components [1]. Moreover, the increasing interest on GAGs and dextran sulfate (DS) due to their structural similarity and anti-viral activity [2,3], as well as good applicability in gene delivery systems [1,4,5], have promoted the development of GAGs as drugs. GAG–lipid interactions are fundamental to understand both their physicochemical behaviour and their pharmacological properties.

* Corresponding authors. Tel.: +358 9 451 2570/2579; fax: +358 9 451 2580.
E-mail addresses: helder.santos@hut.fi (H.A. Santos), kontturi@cc.hut.fi (K. Kontturi).

0022-0728/$ - see front matter © 2006 Elsevier B.V. All rights reserved.
doi:10.1016/j.jelechem.2006.01.024

In our previous work, we showed that DS adsorbs on phospholipid monolayers at air–liquid and liquid–liquid interfaces, and the adsorption is strongly dependent on (i) the surface pressure, (ii) the applied potential, and (iii) the charge of the phospholipid headgroup, enhanced by the presence of calcium ions in the aqueous phase [6]. Furthermore, polyelectrolyte (PE)–metal nanoparticle (NP) self-assembled multilayers deposited on a lipid–DS monolayer can be used to fabricate nanocomposites and nanopatterning materials fundamental for delivery devices [7]. Continuing this work on the interactions between lipid monolayers and water-dispersible metal NP systems that could be used in pharmacology, our current interest is the self-assembly of ruthenium (Ru) NPs using biomolecules (such as DS) as templates. Ru NPs are considered because of the well-known catalytic activity of Ru [8–11], and because positively charged Ru NPs were recently prepared in aqueous medium, providing new opportunities for the surface functionalization with biological ligands such as PEs, DNA and oligonucleotides [12].

In the present work, novel interfacial nanostructures formed by adsorption of composite nanoclusters on a lipid monolayer at the interface between two immiscible electrolyte solutions (ITIES) are characterized electrochemically in relation to their potential use in drug delivery systems. The composite nanoclusters are well-defined and organized structures, as observed under the transmission electron microscope, which are self-assembled in aqueous solution from positively charged Ru NPs and negatively charged DS, which adsorbs on their surface. Langmuir–Blodgett (LB) technique is used to deposit 1-palmitoyl-2-oleoyl-*sn*-glycero-3-phosphatidylcholine (POPC) or 1-palmitoyl-2-oleoyl-*sn*-glycero-3-phospho-*rac*-(1-glycerol) (POPG) monolayers onto an aqueous-organic gel interface at surface pressures of 32, 40, and 47 mN/m in the absence and presence of composite nanoclusters. Thus, we can analyze the influence of the charge of the polar headgroup and the nature of the fatty acid chain. The interaction between the composite nanoclusters and the lipid monolayers is studied by employing alternating current (ac) voltammetry because the interfacial capacitance deduced from these measurements is a very sensitive indicator of dielectric properties and charge distribution [6,7,13–18].

Finally, and building on previous liquid–liquid electrochemistry studies on membrane activity and phase transfer of ionic drugs [13,15,19,20], the transfer mechanism of a cationic Alzheimer drug, 9-amino-1,2,3,4-tetrahydroacridine hydrochloride (tacrine), and a therapeutic anti-infective dye drug, 9-aminoacridine hydrochloride (aminacrine) is studied by cyclic voltammetry.

2. Theory

The interfacial nanostructure under study is depicted in Fig. 1. Phospholipids (POPC or POPG) are deposited as a monolayer at the ITIES. The organic phase contains a concentration c_o^b of a 1:1 electrolyte and the aqueous phase contains a concentration c_w^b of a 2:1 electrolyte. The interfacial nanostructure is described by using a one-dimensional model in which the ITIES is located at the plane $x = 0$, the organic gel occupies the region $x < 0$, and the aqueous solution the region $x > 0$. The organic and aqueous bulk phases have relative electrical permittivities ε_o and ε_w, respectively.

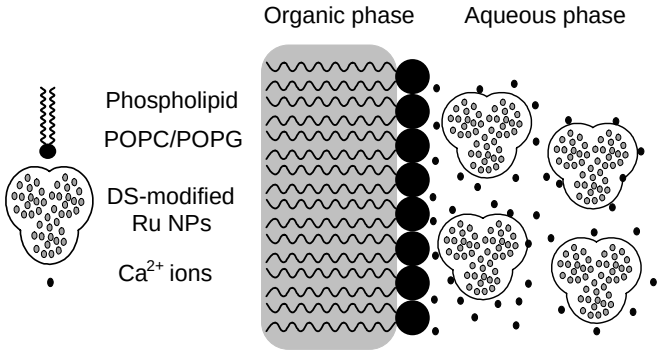

Fig. 1. Schematic representation of the components of the interfacial nanostructure under study. The DS modified Ru NPs are referred as composite nanoclusters. Calcium ions provide stability to the negatively charged POPG headgroups and remain in the close vicinity of the negative DS chains that form the outer shell of the composite nanoclusters.

The hydrocarbon chains of the phospholipids occupy the region $d_{hc} < x < 0$, which is characterized by a relative permittivity ε_{hc}. The different permittivity of the hydrocarbon region and the organic phase implies that a chemical partition coefficient K_{hc} needs to be included when describing the spatial distribution of the organic base electrolyte, and hence its effective concentration in the hydrocarbon region is $c_{hc}^b = K_{hc} c_o^b$. The adsorbed composite nanoclusters occupy the region $0 < x < d_m$, which has an effective relative permittivity ε_m. Again, partitioning effects are important and the effective concentration of the aqueous base electrolyte in this region is $c_m^b = K_m c_w^b$, where K_m is their chemical partition coefficient.

The charges bound to this interfacial nanostructure are modelled as two plane distributions at $x = 0$ and $x = d_m$ (see Fig. 2). The respective electrical charge densities are σ_0 and σ_m or, in dimensionless units, $\alpha \equiv A\sigma_0/e$ and $\gamma \equiv A\sigma_m/e$ where e is the elementary charge and A is the mean molecular area of the phospholipids in the monolayer.

Using this simplified model of the interfacial nanostructures and Poisson–Boltzmann theory [6,7,16] we evaluate first the capacitance C defined as

$$C \equiv \frac{\partial Q}{\partial \Delta_o^w \phi} \qquad (1)$$

where Q is the charge density separated across the ITIES and $\Delta_o^w \phi \equiv \phi_w^b - \phi_o^b$ is the Galvani potential difference between the bulk aqueous and organic phases. The electric potential distribution is described by the Poisson–Boltzmann equation:

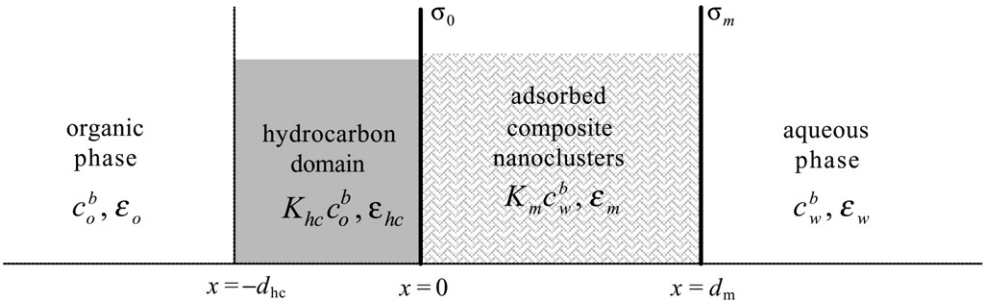

Fig. 2. Simplified view of the interfacial nanostructure as a four layer system with surface charge distributions σ_0 and σ_m at the ITIES and the external boundary of the adsorbed layer of composite nanoclusters, respectively.

$$\frac{d^2\varphi}{dx^2} = \kappa_o^2 \sinh\varphi; \quad x < d_{hc} \tag{2a}$$

$$\frac{d^2\varphi}{dx^2} = \kappa_{hc}^2 \sinh\varphi; \quad d_{hc} < x < 0 \tag{2b}$$

$$\frac{d^2\varphi}{dx^2} = \kappa_m^2 \sinh(\varphi - \Delta_o^w\varphi) e^{2(\varphi - \Delta_o^w\varphi)}; \quad 0 < x < d_m \tag{2c}$$

$$\frac{d^2\varphi}{dx^2} = \kappa_w^2 \sinh(\varphi - \Delta_o^w\varphi) e^{2(\varphi - \Delta_o^w\varphi)}; \quad d_m < x \tag{2d}$$

where φ is the electric potential in RT/F units and measured with respect to the bulk organic phase,

$$\kappa_i \quad \frac{2F^2 c_i^b}{\varepsilon_i \varepsilon_0 RT}^{1/2} \tag{3}$$

is the Debye parameter in region i ($i = o, hc, m, w$), and ε_0 is the vacuum electrical permittivity. The boundary conditions for the electric displacement are

$$\varepsilon_o \frac{d\varphi}{dx}_{x=d_{hc}} = \varepsilon_{hc} \frac{d\varphi}{dx}_{x=d_{hc}^b} \tag{4a}$$

$$\varepsilon_{hc} \frac{d\varphi}{dx}_{x=0^-} = \varepsilon_m \frac{d\varphi}{dx}_{x=0^+} + \frac{F\sigma_0}{\varepsilon_0 RT} \tag{4b}$$

$$\varepsilon_m \frac{d\varphi}{dx}_{x=d_m} = \varepsilon_w \frac{d\varphi}{dx}_{x=d_m^b} + \frac{F\sigma_m}{\varepsilon_0 RT} \tag{4c}$$

$$Q \quad \int_1^0 \rho\, dx = \frac{2\varepsilon_0 RT}{F} \left(\kappa_o^2\varepsilon_o^2 \quad \kappa_{hc}^2\varepsilon_{hc}^2 \right) \sinh^2\frac{\varphi(d_{hc})}{2} + \kappa_{hc}^2\varepsilon_{hc}^2 \sinh^2\frac{\varphi(0)}{2}^{1/2} \tag{5}$$

and the interfacial capacitance $C = F/RT \cdot dQ/d\Delta_o^w\varphi$ is calculated by numerical differentiation; note that Eq. (5) was incorrectly written in Refs. [6,7], although the results obtained thereof are correct and not affected by this typographical error.

3. Experimental

3.1. Materials

The chemicals POPC from egg yolk type XVI-E (Sigma, 99%), POPG (Sigma, 99%), 2-nitrophenyl octyl ether (*o*-NPOE, Fluka, Selectophore), poly(vinyl chloride) (PVC, Sigma, very high molecular weight), chloroform (Merck, PA), tetraphenylarsonium chloride hydrate 97% (TPAsCl, Sigma, PA), tetrakis-4-chlorophenylborate (KTPBCl, Aldrich, PA), calcium chloride ($CaCl_2$, Merck, PA), ruthenium (III) chloride hydrate ($RuCl_3$, Aldrich, 99.98%), sodium borohydrate ($NaBH_4$, Merck, for synthesis), sodium hydroxide pellets (NaOH, Merck, reagent grade), tacrine (Sigma, reagent grade), aminacrine (Sigma, minimum 98%) and DS sodium salt from Leuconostoc ssp. (DS 500, Fluka, 500 kDa) were all used as received without further purification. Millipore Milli-Q water (resistivity > 18 MΩ cm) was used to prepare all aqueous solutions and for rinsing. Fig. 3 shows the chemical structure of DS and the drugs used.

3.2. Preparation and characterization of composite nanoclusters

The preparation of positively charged Ru NPs was based on Ref. [12] with slight modifications. Briefly and first, the Ru hydrosol was prepared by introducing dropwise 0.1 M $NaBH_4$ aqueous solution into 10 mL of 2 mM $RuCl_3$ aqueous solution under vigorous stirring. During

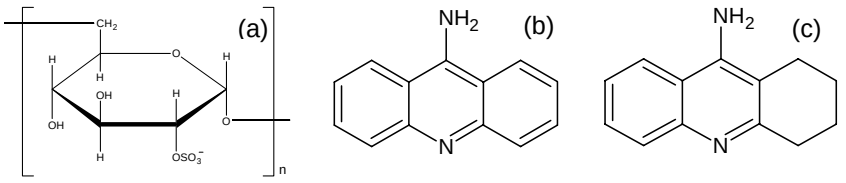

Fig. 3. Molecular structures of (a) DS, represented in one of the three possible sulfate group forms, (b) aminacrine, and (c) tacrine, the latter two in their neutral forms.

the addition the pH was kept lower than 4.9 and the positive charge of the NPs was confirmed by zeta (ζ)-potential measurements. By mixing 10 mL of a 1 mg/mL DS aqueous solution, 10 mL of an aqueous solution of Ru hydrosol, and 120 μL of 1 M NaOH aqueous solution (to neutralize the hydrated protons), a dark-brown transparent solution with no precipitates was obtained. UV–vis spectroscopy and transmission electron microscopy (TEM) confirmed the self-assembling of well-defined and organized structures that are referred to as composite nanostructures. Finally, an aqueous solution of 3 mM $CaCl_2$ and composite nanoclusters was prepared. The pH of the final solution used in all experiments was about 6.6.

The size distribution of the Ru hydrosol and the composite nanoclusters was confirmed using a TEM (Tecnai G2, operating at 120 kV with 0.5 nm point resolution) and free software, Image J. The samples were prepared by adding droplets of an aqueous solution of Ru hydrosol or composite nanoclusters on the copper–carbon grids and leaving them in a dry box for ca. 24 h.

The ζ-potentials of aqueous solutions of Ru hydrosol and composite nanoclusters were measured using a NICOMP™ ζ-potential/particle sizer 380 ZLS (Santa Barbara, CA, USA) with the following parameters settings: wavelength 632.8 nm, medium viscosity 0.933 cP, medium refraction index 1.333, scattering angle 14.7°, medium relative permittivity 78.50, and electric field strength 10.00 V/cm. The measurements were repeated at least three times.

3.3. Langmuir–Blodgett films

POPC and POPG solutions were dissolved in chloroform and used as spreading solutions. The typical solutions concentration used was 1 mg/ml. Surface pressure–molecular area (π–A) isotherms were measured with a computer-interfaced Langmuir trough (length 300 mm, width 150 mm, KSV Instruments Ltd., Helsinki) housed in an earthed Faraday cage. The subphase temperature was maintained constant at 20.0 ± 0.1 °C. Lipid solutions (ca. 26 μL) were spread onto an aqueous subphase of 3 mM $CaCl_2$ containing DS-modified Ru NPs, with a typical ratio of 1:45 (DS relatively to Ru) with a Hamilton syringe. The isotherms were then recorded after the solvent has evaporated (30 min) with the compression speed of 5.0 mm min^{-1}. LB films were transferred by dipping the electrochemical cell perpendicularly through the lipid monolayer as described elsewhere [15,16]. The deposition speed was 2.0 mm min^{-1}. The success of the transfer was determined both from the electrochemical measurements and the so-called transfer ratio, with values close to unit. The surface pressures studied in this work were 32, 40, and 47 mN/m. No changes in the monolayer properties were observed over several hours even after deposition.

3.4. Electrochemical measurements

Ac and cyclic voltammetry measurements were carried out using a four-electrode apparatus system and an electrochemical cell. The cell was made of poly(tetrafluoroethylene) with an interfacial area of 0.28 cm^2. For the preparation of the organic gel phase a mixture of 5 wt% PVC and *o*-NPOE containing the base electrolyte was heated at least to 110 °C, and the resulting hot gel was simply cast into the cell. Typically, the solidification of the gel was carried out overnight. $CaCl_2$ was used as aqueous base electrolyte and TPAsCl as the organic reference electrolyte. The organic base electrolyte TPAsTPBCl was obtained by precipitation from equimolar solutions of TPAsCl and KTPBCl [21]. Ag/AgCl reference electrodes were used for the electrochemical measurements and the auxiliary electrodes were Pt wires.

The electrochemical cell is represented in Scheme 1, where X is either tacrine or aminacrine. The cell interface was positioned between two Luggin capillaries to minimize the ohmic drop. All electrochemical experiments were carried out inside of a grounded Faraday cage with the Autolab® PGSTAT100 (EcoChemie B.V., Netherlands) at 20.0 ± 0.1 °C. Ac voltammetry was measured at 5, 10, 20, 25, and 30 Hz, using a sweep rate of 1 mV s^{-1}, an amplitude of 5 mV root-mean-square, with a modulation and interval time of 0.4 and 1 s, respectively.

4. Results and discussion

4.1. Characterization of the phospholipid monolayers

In Fig. 4, the π–A isotherms of POPC (a) and POPG (b) monolayers at 20.0 ± 0.1 °C spread on an aqueous subphase of Ca^{2+} in the absence (solid line) and presence (dashed line) of composite nanoclusters are shown. At the pH of the measurements, the headgroups are zwitterionic in the case of POPC and negatively charged in the case of POPG. The two phospholipids form stable monolayers at an air–liquid interface. The compression isotherms are smooth without structural transitions. Both isotherms are characteristic for a homogeneous liquid expanded state. At a surface pressure of ca. 48 and 50 mN/m corresponding to mean molecular areas of ca.

			10 mM TPAsTPBCl	3 mM $CaCl_2$		
Ag	AgCl	5mM TPAsCl	5wt-% PVC	+ DS-Ru NPsX	AgCl	Ag'
		(w')	(o-NPOE)	(w)		

Scheme 1.

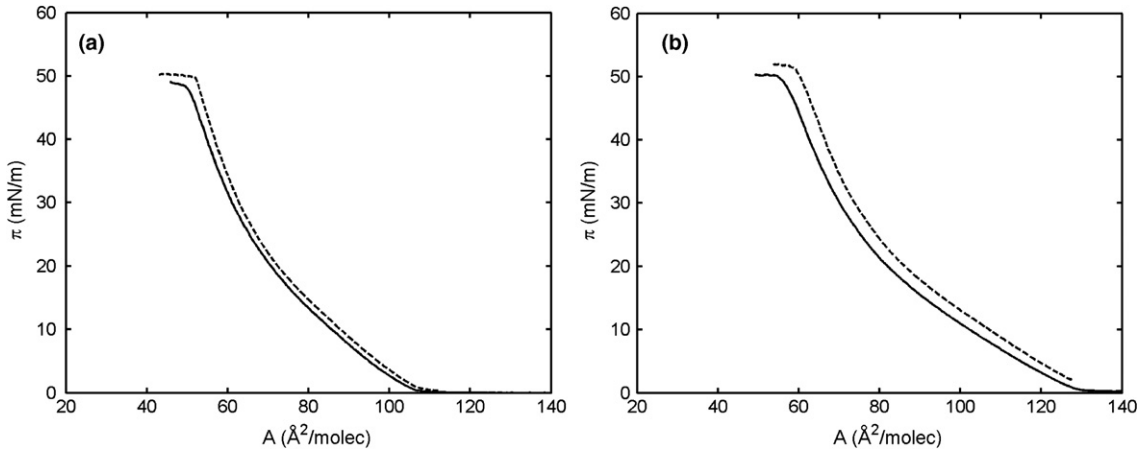

Fig. 4. The isotherms measured at 20.0 ± 0.1 °C for POPC (a) and POPG (b) monolayers at an air–aqueous interface spread on 3 mM Ca^{2+} aqueous subphase in the absence (solid line) and presence (dashed line) of composite nanoclusters.

50 and 55 $Å^2$ the films for POPC and POPG, respectively, collapsed. The isotherm of POPG is more expanded even without the adsorption of nanoclusters. In the presence of composite nanoclusters in the subphase, the isotherms shift towards larger areas per molecule (ca. 52 and 58 $Å^2$ for POPC and POPG, respectively) and the monolayers collapse at slightly higher pressures (ca. 50 and 51 mN/m for POPC and POPG, respectively). Furthermore, the adsorption of the composite nanoclusters to the lipid monolayer leads to slightly expanded isotherms, as it should be expected from their charged headgroups. The results also show no penetration of the composite nanostructures into the lipid monolayer, because no increase of the surface pressure at larger molecular areas was observed [6,7]. Hence, it is suggested that the negatively charged composite nanoclusters are attached electrostatically to the lipid headgroups via Ca^{2+} ions (as suggested in Fig. 1), and thus adsorbed at the interface only. Ca^{2+} mediates the interactions between the lipids and the composite nanoclusters leading to the formation of lipid/Ca^{2+}/composite nanuclusters complexes. This leads to the formation of very organised and rigid monolayers, which are responsible for the shape of the isotherms.

4.2. Characterization of the composite nanoclusters

It has been shown that hydronium ions or other hydrated protons (the adsorbed species on NPs surface) make the surface of Ru NPs positively charged [12]. The charged Ru NPs can be used to build different nanoscale Ru clusters or protecting agents as well as to coordinate biological ligands. The latter case is considered here.

In the present study, we describe a novel nanostructure system, which is self-assembled in an aqueous solution from positively charged Ru NPs and negatively charged DS. Their size distribution, charge, and morphology were subsequently studied. For that purpose, the Ru hydrosol and the negatively charged composite nanoclusters were characterized by UV–vis and TEM spectroscopy, and ζ-potential measurements. TEM images of the composite nanoclusters are shown in Fig. 5a and b. Fig. 5c also shows the particle size distribution and the UV–vis spectra for the Ru solution (solid line), Ru hydrosol (dashed line), and composite nanoclusters (dashed line). The average size of positively charged Ru NPs was ca. 1.6 nm (results not shown). The positive charge on the Ru NP surface was confirmed by ζ-potential measurements. The mean ζ-poten-

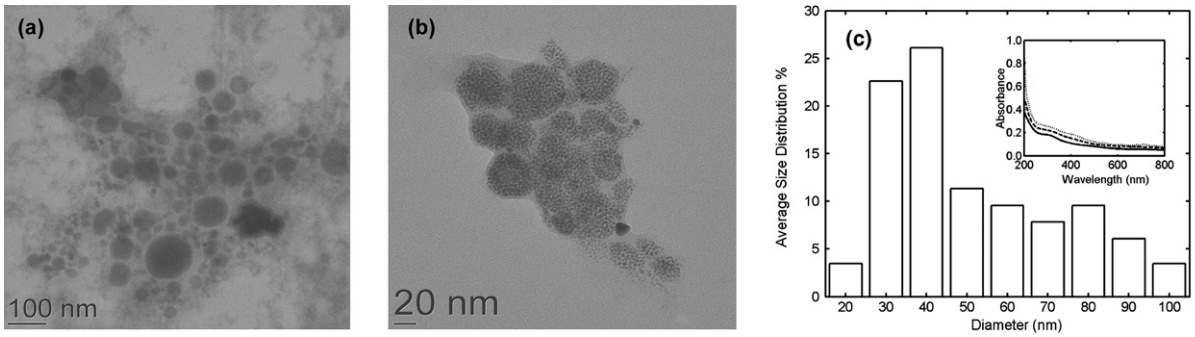

Fig. 5. (a) TEM image of the composite nanoclusters (DS-modified Ru NPs), and (b) magnification of an aggregate of nanoclusters. The average size of the nanoclusters is ca. 40 nm; the average size of the Ru NPs is ca. 1.6 nm (size distribution not shown). (c) Size distribution of the composite nanoclusters, and UV–vis spectra (inset) of Ru solution (solid line), Ru hydrosol (dashed line), and composite nanoclusters (dotted line).

tial of +50.40 mV clearly indicates that the Ru surface was positively charged. The results are in very good agreement with the literature [12].

The UV–vis spectra showed adsorption band with λ_{max} at ca. 300 nm for Ru (brown solutions were observed). The surface plasmon band is almost imperceptible for the composite nanoclusters (maybe due to the very dilute solutions used), and their absorbance increases when compared with that of the Ru hydrosol, and more significantly at high energies, due to both their larger size and the presence of DS on the surface. As it was stated before, Ru NPs are stabilized electrostatically by means of the low pH used (pH < 4.9). After DS addition, Ru NPs are surrounded by DS and form clusters of individual Ru NPs with a size of approximately 1.6 nm (the average diameter of DS + Ru NPs is then ca. 40 nm). DS only is not optical active, and therefore the UV–vis spectra of composite nanoclusters does not exhibit significant differences in the absorbance relatively to that of Ru NPs only, because both are due to the presence of Ru NPs, which also indicates adequate dispersion of Ru NPs within the biopolymer, containing each nanocluster approximately the same amount of Ru NPs (see also Fig. 5a and b).

In Fig. 5a and b composite nanoclusters show particles with a spherical shape and a smooth surface with an average diameter of ca. 40 nm, that can be identified as well-defined constituents of the aggregate. These self-assembled nanoclusters are negatively charged (ζ-potential of 36.44 mV), which clearly indicates that the DS chains are on the surface of the Ru NPs. The presence of Ca^{2+} ions is also very important for the formation of these composite nanoclusters, due to the interaction between Ca^{2+} ions and DS. As a result of this interaction, Ca^{2+} can link to two DS chains, which increases the number of particles per cluster. As a consequence, larger clusters are observed in the TEM pictures.

Finally, it should be stressed that, Ru nanoparticles solutions were only stable for a short period of time, contrarily to that state elsewhere [12]. Nevertheless, the composite nanostructure (DS-modified Ru NPs) solutions prepared this way were very stable, and no precipitation was observed even after storage over one month.

4.3. Interfacial capacitance

The interaction between the composite nanoclusters and the phospholipid monolayers was studied by interfacial capacitance obtained from ac voltammetry. Assuming that the transfer of the base electrolyte ions is diffusion controlled, and the ohmic solution resistance completely compensated, the equivalent electric circuit can be modelled as the parallel combination of a capacitor and a Warburg impedance. Therefore, the experimental capacitance can be determined as [22], $C = (Y^{00} \quad Y^{0})/\omega$, where $Y^{00}$and Y^{0} are the imaginary and the real components of a measured total admittance, respectively, and ω is the angular frequency of the ac signal. Fig. 6a–d show the capacitance as a function of the Galvani potential difference for monolayers deposited at surface pressures of 32, 40 and 47 mN/m.

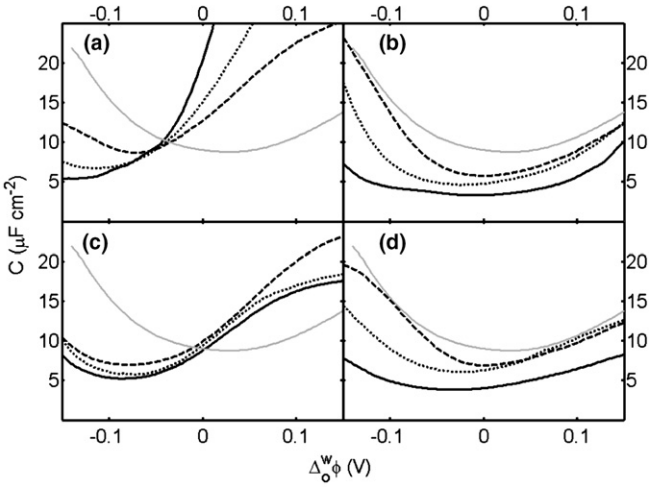

Fig. 6. Measured capacitance versus potential curves of POPC (a, c) and POPG (b, d) monolayers deposited on the aqueous–organic gel interface in the absence (a, b) and in the presence (c, d) of composite nanoclusters. The surface pressures are 32 (dashed line), 40 (dotted line), and 47 mN/m (solid line). The curve for a bare interface (solid, gray line) is also shown for comparison.

Fig. 6a and b show the measured capacitance in the absence of composite nanoclusters in the aqueous solution. In the case of POPC (Fig. 6a) the interfacial capacitance is lower than for the bare interface at negative potentials and higher at positive potentials. As the surface pressure increases, this effect becomes more marked and the minimum of the interfacial capacitance shifts towards more negative potentials. In the case of POPG (see Fig. 6b), the interfacial capacitance is always lower than for the bare interface, which indicates that the phospholipids are strongly adsorbed at the interface over all the potentials and surface pressures considered.

Fig. 6c and d show the measured capacitance in the presence of composite nanoclusters. A different trend in the capacitance is now observed for both lipids compared with those in Fig. 6a and b. In the case of POPC (see Fig. 6c) the interfacial capacitance at more positive potentials is lower compared to that in the absence of composite nanoclusters (this change is more noticeable in the curve corresponding to 47 mN/m). The minima of the capacitance curves are again located at more negative potentials than for the bare interface but no significant shift with increasing surface pressure is now observed. This may be due to the formation of a more rigid interfacial nanostructure when the composite nanoclusters are adsorbed on the POPC monolayer. In the case of POPG (see Fig. 6d), the minima of the capacitance curves is now shifted towards more negative potentials as the surface pressure is increased. Comparing these capacitance curves to those in the absence of the lipid monolayer, different trends can be observed in the capacitance curves of only composite nanoclusters (results not shown). The main trends are: (i) shifts the minimum to

more positive potentials; (ii) increases slightly the capacitance at low potentials, with values higher than for the bare interface due to the presence of DS [6]; and (iii) increases the value of the minimum capacitance compare to those in the presence of lipid.

In the theoretical model used to calculate the simulated capacitance curves the relative permittivities of the bulk phases are $\varepsilon_o = 24.2$ and $\varepsilon_w = 78.54$ [7], the parameters ε_{hc} and α are allowed to vary, and the other parameters are kept constant as $d_{hc} = 1.1$ nm, $K_{hc} = 0.4$, $d_m = 40$ nm, $K_m = 2$, and $\gamma = 0.06$. The values of ε_{hc} and α used to calculate the capacitance curves are shown in Table 1. Their variation with the surface pressure is as follows. As observed in a previous work [6] and confirmed here, an increase in the surface pressure of the phospholipid monolayer lowers the effective dielectric constant of the hydrocarbon domain and decreases the capacitance minimum. Parameter α describes the effective surface charge density at the ITIES and is expected to increase when the monolayer is compressed and becomes more compact (increasing the capacitance at positive potentials) in the absence of composite nanoclusters.

Fig. 7a shows the capacitance curves for a POPC monolayer in the absence of composite nanoclusters calculated from the solution of Eqs. (1)–(5). Since the headgroups are zwitterionic at the pH 7 of the measurements, the fact that the minimum of the capacitance curves lies at negative potentials is interpreted as an evidence of calcium binding [6]. When the surface pressure is increased, the minimum capacitance slightly decreases, and this is attributed to a decrease of the effective dielectric constant of the hydrocarbon domain. The large increase of the capacitance at more positive potentials with respect to the bare interface and its increase with the surface pressure are correctly reproduced by the predictions of the theoretical model. This is due to the increased surface charge density with compression as the pressure increases. This higher value for the surface charge density (α positive and increasing with π) explains also the slight shift of the minima to more negative potentials and confirms the expectation above made.

Fig. 7c shows the calculated capacitance curves of POPC monolayers in the presence of composite nanoclusters. As it should be expected from their negative charge, the adsorption of the nanoclusters decreases α and shifts slightly the minima of the capacitance curves to more positive potentials. The shift, however, is not as remarkable as the fact that the capacitance at positive potentials now decreases with increasing pressure. This latter observation is also related to the lower values of α.

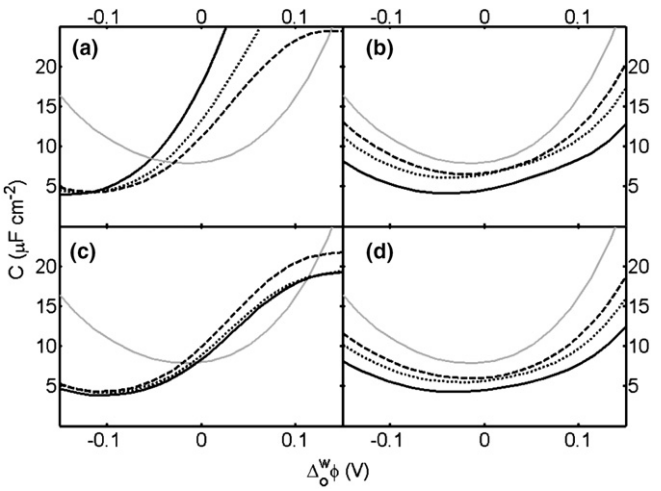

Fig. 7. Calculated capacitance curves of POPC (a, c) and POPG (b, d) monolayers at the aqueous–organic gel interface in the absence (a, b) and in the presence (c, d) of composite nanoclusters. The surface pressures are 32 (dashed line), 40 (dotted line), and 47 mN/m (solid line). The curve for a bare interface (solid, gray line) is also shown for comparison.

Since the POPG headgroups are negatively charged [6] the capacitance minima are located at more positive potentials (see Fig. 7b and d) than in the case of POPC. The effective surface charge density α is positive due to the binding of calcium ions (necessary for the subsequent adsorption of the composite nanoclusters) but much lower than for the zwitterionic POPC. The adsorption of the negatively charged composite nanoclusters decreases further the value of the effective surface charge density α at the ITIES. This explains the slight shift to more positive potentials of the minima in Fig. 7d with respect to those in Fig. 7b.

In conclusion, all the experimental observations are satisfactorily described by the theoretical model. As it has been observed previously [6,7], the agreement is only qualitative because this type of theoretical models overestimates the capacitance at high (positive) potential differences and underestimates it at low (negative) potential differences. However, the information provided by this modelling on the interactions taking place is judged to be correct.

Table 1
Parameter values used in the calculations of capacitance curves for POPC and POPG, minimum capacitance, at different pressures and in absence and presence of composite nanoclusters

	π (mN/m)	ε_{hc}	α (absence)	α (presence)	$C_{min.cap.}$/μF cm $^{-2}$ (absence)	$C_{min.cap.}$/μF cm $^{-2}$ (presence)	δ
POPC	32	3.6	0.10	0.09	8.67	6.98	0.018
	40	3.45	0.125	0.08	6.73	5.77	0.02
	47	3.35	0.18	0.08	5.32	5.24	0.06
POPG	32	15	0.01	0.003	5.74	6.87	0.005
	40	10	0.02	0.012	4.61	6.07	0.01
	47	4	0.02	0.012	3.30	3.84	0.01

Shifts of the capacitance minimum $\delta = \Delta_o^w\phi_{min.cap.}^{(presence)} - \Delta_o^w\phi_{min.cap.}^{(absence)}$ are also tabulated. As it should be expected, the adsorption of negatively charged composite nanoclusters lowers the value of α.

4.4. Drug transfer

The transfer of ionic drugs across the interfacial nanostructures was studied by cyclic voltammetry. The selected compounds (aminacrine and tacrine, see Fig. 3) have at least one protonation/deprotonation site and are of great relevance in pharmacology. Tacrine is an acetylcholinesterase inhibitor drug used in the treatment of Alzheimer's disease and aminacrine is a therapeutic anti-infective dye drug. Their pK_a values are similar: 9.99 and 9.8 for aminacrine and tacrine, respectively [23]. According to Mälkiä et al. [13], aminacrine and tacrine adsorb in the hydrocarbon tail region of the monolayer as well as on the lipid headgroups, and thus increase their ability to pass through biological and biomimetic membranes. Typical cyclic voltammograms (CVs) of aminacrine (a, c) and tacrine (b, d) transfer recorded at different scan rates in the absence (a, b) and presence (c, d) of POPC monolayers deposited on the ITIES at surface pressure of 40 mN/m in the presence of composite nanoclusters in the subphase are shown in Fig. 8. Similar results were obtained for POPG (results not shown). Each voltammogram was corrected for the current due to the supporting electrolytes only.

The first observation which can be made from the voltammograms is the shift of the voltammetric waves. The half-wave potential of aminacrine is 58 mV at the bare interface (CV not shown), 22 mV in the presence of nanoclusters (Fig. 8a), 100 mV in the presence of lipid monolayer (CV not shown), and 79 mV in the presence of them both (see Fig. 8c). This shows that aminacrine is adsorbed on both the nanoclusters and the lipid monolayer. The shape of the forward peaks in Fig. 8a, where the nanoclusters are present, is a bit distorted, reminding of a dissolution type of behaviour. Apparently, positively charged aminacrine is bound on negatively charged clusters rather tightly via electrostatic interaction, as also confirmed by the shift of +36 mV in the half-wave potential. Adsorption on the lipid monolayer is even more pronounced, as indicated by the shift of 42 mV in the presence of the monolayer and of 21 mV in the presence of both of them. In Fig. 8a, the peak separation varies from 45 to 75 mV and this suggests mixed adsorption, diffusion and kinetic control of aminacrine transfer. A quantitative analysis in terms of, e.g., rate constants via Nicholson–Shain theory is impossible without additional information of adsorption constants. In Fig. 8c the peak separation remains practically the same, at ca. 40 mV, indicating mixed diffusion and adsorption control, i.e., adsorption shadows the kinetics of ion transfer.

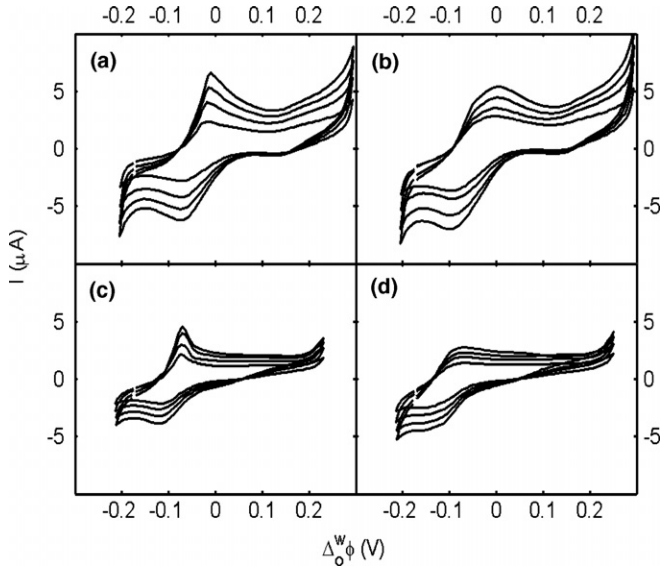

Fig. 8. CVs of aminacrine (a, c) and tacrine (b, d) transfer recorded at scan rates of 25, 50, 75, and 100 mV/s (from bottom to top) in the absence (a, b) and presence (c, d) of POPC monolayers deposited on the aqueous–organic gel interface at a surface pressure of 40 mN/m in the presence of composite nanoclusters in the subphase. The typical drug concentration was ca. 50 μM.

In Fig. 8b for tacrine in the presence of nanoclusters, two separate peaks in forward direction can be seen. The peaks overlap each other so closely that at slow scan rates only one broad peak is visible. The peak separation between the first forward and the backward peak is ca. 60 mV, while between the second forward and the backward one the separation varies between 100 and 110 mV. In Fig. 8d, an accurate determination of the peak separation is rather difficult, but an estimate of 55–60 mV can be given. The existence of two peaks in Fig. 8b confirms further that also tacrine is adsorbed on the nanoclusters, and that its transfer kinetics across the ITIES is slower that of aminacrine. Also the half-wave potential of transfer is shifted by ca. 30 mV in the presence of the monolayer.

The peak currents are suppressed ca. 30% in the case of aminacrine and by ca. 45% in the case of tacrine. At the surface pressure of 40 mN/m corresponding to the mean molecular area of ca. 57 Å^2 the surface coverage of the lipid is ca. 0.9, if it is assumed that the collapse at 50 mN/m and 52 Å^2/molecule corresponds to the full coverage. If the ion transfer took place only through the openings between the lipid domains [24], the current suppression would be much larger. It can be thus estimated that the lipid layer retards the rate of ion transfer by a factor of 2/3 (60%:90%) in the case of aminacrine and by a factor of 1/2 (45%:90%) in the case of tacrine.

In summary, as it was demonstrated previously [17] also here the rate ion transfer decreases as the surface pressure increases (results not shown). However, in the presence of these composite nanoclusters this effect seems to be rather evident, and independent of the phospholipid headgroup.

5. Conclusions

Negatively charged composite nanoclusters were prepared by self-assembling of DS chains and Ru NPs in aqueous medium and observed under TEM as well-defined and organized structures. These nanoclusters were then used for studying their interaction with phospholipid monolayers deposited on a liquid–liquid interface using

LB and electrochemical techniques. By comparing the measured and calculated capacitance–potential curves, and with the help of a theoretical model, the charge distribution in the interfacial nanostructures formed by the phospholipid monolayers and adsorbed composite nanoclusters was elucidated. In general, a decrease of the capacitance minimum (which indicated a lower relative permittivity of the hydrocarbon region) and a shift to more negative potentials (which indicated an increase in the surface charge density α) was observed for the monolayer when the surface pressure was increased. Drug transfer across these interfacial nanostructures was then studied by cyclic voltammetry. It was demonstrated that the lipid layer retards the rate of ion transfer by a factor of 2/3 and 1/2 in the case of aminacrine and tacrine, respectively.

The interactions of these NPs with natural and artificial membranes and their potential use in drug delivery systems are of interest in biological studies. For example, in the system presented, a lipid monolayer serves as an in vitro model for a plasma membrane. Since the NPs also tune the permeability properties of the membranes, GAG-modified NPs are used in several drug formulations to tune the release rate of the drug from the formulation. Therefore, this system mimics the interaction of such formulations with the plasma membrane. Moreover, NPs can be used to direct the formulation into the target tissue. This can be accomplished with the magnetic field if the NPs are magnetic. Ru NPs are not magnetic, but their catalytic properties can be utilized in various redox reactions taking place in the tissues when in contact with a NP-containing formulation.

Acknowledgments

Financial support from European Union under the research and training network SUSANA (“Supramolecular Self-Assembly of Interfacial Nanostructures”, Contract Number HPRN-CT-2002-00185) is gratefully acknowledged. H.A. Santos thank Timo Laaksonen for technical assistance with TEM images and Marjo Männistö (Department of Pharmaceutics, University of Kuopio, Finland) for all the help with ζ-potential measurements. J.A.M. and V.G.M. acknowledge financial support from the DGICYT (Ministry of Education and Science of Spain) and the FEDER funds of the European Union through Project Number MAT2002-0646.

References

[1] M. Ruponen, S. Ylä-Herttuala, A. Urtti, Biochim. Biophys. Acta 1415 (1999) 331.
[2] B. Radhakrishnamurthy, H.A. Ruitz, S.R. Srinivasan, W. Preau, E.R. Dalferes, G.S. Berenson, Atherosclerosis 31 (1978) 217.
[3] A.D. Bangham, M.W. Hill, N.G.A. Miller, Science 240 (1988) 646.
[4] M. Ruponen, P. Honkakoski, M. Tammi, A. Urtti, J. Gene Med. 6 (2004) 405.
[5] C. Wiethoff, J.G. Smith, G.S. Koe, C.R. Middaugh, J. Biol. Chem. 276 (2001) 32806.
[6] H.A. Santos, V. García-Morales, R.-J. Roozeman, J.A. Manzanares, K. Kontturi, Langmuir 21 (2005) 5475.
[7] H.A. Santos, M. Chirea, V. García-Morales, F. Silva, J.A. Manzanares, K. Kontturi, J. Phys. Chem. B 109 (2005) 20105.
[8] O. Solorza-Feria, S. Durón, Int. J. Hydrogen Energy 27 (2002) 451.
[9] A. Miyazaki, I. Balint, K.-I. Aika, Y. Nakano, J. Catal. 204 (2001) 364.
[10] I. Balint, A. Miyazaki, K.-I. Aika, J. Catal. 207 (2002) 66.
[11] I. Balint, A. Miyazaki, K.-I. Aika, Chem. Commun. (2002) 630.
[12] J. Yang, J.Y. Lee, T.C. Deivaraj, H.-P. Too, J. Colloid Interf. Sci. 271 (2004) 308.
[13] A. Mälkiä, P. Liljeroth, K. Kontturi, Electrochem. Commun. 5 (2003) 473.
[14] A. Mälkiä, P. Liljeroth, K. Kontturi, Anal. Sci. 17 (2001) i345.
[15] A. Mälkiä, P. Liljeroth, A.-K. Kontturi, K. Kontturi, J. Phys. Chem. B 105 (2001) 10884.
[16] P. Liljeroth, A. Mälkiä, V. Cunnane, A.-K. Kontturi, K. Kontturi, Langmuir 16 (2000) 6667.
[17] A. Mälkiä, P. Liljeroth, K. Kontturi, Chem. Commun. (2003) 1430.
[18] H.A. Santos, C.M. Pereira, F. Silva, Port. Electrochim. Acta 23 (2005) 263.
[19] F. Reymond, P.-A. Carrupt, B. Testa, H.H. Girault, Chem. Eur. J. 5 (1999) 39.
[20] K. Kontturi, L. Murtomaki, J. Pharm. Sci. 81 (1992) 970.
[21] V.J. Cunnane, D.J. Schiffrin, C. Beltran, G. Geblewicz, T.J. Solomon, Electroanal. Chem. 247 (1988) 203.
[22] T. Kakiuchi, M. Senda, Collect Czech. Chem. Commun. 56 (1991) 112.
[23] C.J. Drayton, in: C. Hansch, P.G. Sammes, J.B. Taylor (Eds.), Comprehensive Medicinal Chemistry, vol. 6, Pergamon Press, Oxford, 1990.
[24] M. Thoma, H. Möhwald, J. Colloid Interf. Sci. 162 (1994) 340.